Structure and Nonrigidity of $B_9H_9^{2-}$ and $B_9H_{10}^-$. Comparisons of $B_nH_n^{2-}$ and $B_nH_{n+1}^-$ Systems

Alexander M. Mebel,[†,‡] Paul von Ragué Schleyer,*[,§] Katayoun Najafian,[§] and Oleg P. Charkin[†]

Institute of New Chemical Problems, Russian Academy of Sciences, Chernogolovka, Moscow region, 142432 Russia, Institut für Organische Chemie der Universität Erlangen-Nürnberg, Henkestrasse 42, D-91054 Erlangen, Germany, and Institute of Atomic and Molecular Sciences, Academia Sinica, P.O. Box 23-166, Taipei, Taiwan

Received July 31, 1997

Ab initio calculations at MP2/6-31G*, B3LYP/6-31G*, and B3LYP/6-311+G** levels indicate relatively high potential barriers for the intramolecular rearrangement of $B_9H_9^{2-}$ via the single DSD (diamond−square−diamond) or the double DSD mechanism, 28.4 and 21.3 kcal/mol, respectively. However, its open face-protonated form, $B_9H_{10}^-$ (**2b**) is highly fluctional. Two other minima, **2a** (C_{2v}) and **2c** (C_{3v}) have energies 1.1 and 9.7 kcal/mol higher than **2b**. Facile rotation of the BH_2 group in **2a** is coupled with reversible opening of the boron cage from the *closo* to a *nido* form. Structure **2c**, with a face-bound proton, is a very shallow minimum along the degenerate rearrangement pathway of **2b**. None of the optimized structures of $B_9H_{10}^-$ give calculated ^{11}B chemical shifts corresponding to experiment; the NMR assignments and interpretation need to be refined. Members of the $B_nH_{n+1}^-$ series ($n = 6-8$, 10, and 12) have both common as well as specific features. All $B_nH_{n+1}^-$ species are fluxional, due to rapid proton migration. The additional hydrogen H* rotates over the whole boron octahedron in $B_6H_7^-$ and over one side of the bipyramid in $B_7H_8^-$. In $B_{10}H_{11}^-$, the "extra" hydrogen H* migrates around the faces of a "polar region" near the apical borons more readily than from pole to the other; as in $B_9H_{10}^-$, H* migration in $B_8H_9^-$ is accompanied by a skeletal rearrangement. The proton affinities (PA) in the $B_nH_n^{2-}$ series decrease with increasing size, since the Coulomb repulsion in the dianions becomes smaller and the coordination number at the protonation sites increases.

Introduction

The structural nonrigidity of *closo*-boranes and carboranes continues to be explored intensively.[1−6] While $B_8H_8^{2-}$ and $B_{11}H_{11}^{2-}$ show fluxional mobility at ambient temperatures,[2] there is no structural ambivalence or experimental evidence for rearrangements of $B_9H_9^{2-}$ (**I**) in solution or in the solid.[2] The X-ray structures of the $B_9H_9^{2-}$ anion with various counterions do not reveal distortions of the polyhedral framework toward geometries which might point to possible rearrangement intermediates. Theoretically, both single and double "diamond−square−diamond" (DSD) mechanisms have been considered (see Figure 1) for the possible reorganization of the boron skeleton in $B_9H_9^{2-}$.[4] The single DSD rearrangement is said to be symmetry-forbidden.[4b] The double DSD process is symmetry-allowed, but since two B−B bonds must be broken it was presumed to involve a high barrier.

Protonation of the $B_nH_n^{2-}$ dianions leads to a new class of $B_nH_{n+1}^-$ monoanions.[7,8] The structures of four members of this family, $B_6H_7^-$, $B_7H_8^-$, $B_8H_9^-$, and $B_{10}H_{11}^-$, were studied earlier using various experimental methods[7] and nonempirical calculations.[9,10] The $B_9H_{10}^-$ anion (**2**) also was synthesized by

[†] Russian Academy of Sciences.
[‡] Academia Sinica.
[§] Universität Erlangen-Nürnberg.

(1) Muetterties, E. L.; Wiersema, R. J.; Hawthorne, M. F. *J. Am. Chem. Soc.* **1973**, *95*, 7520. (b) Muetterties, E. L. *Tetrahedron* **1974**, *30*, 1595. (c) Muetterties, E. L.; Hoel, E. L.; Salentine, C. G.; Hawthorne, M. F. *Inorg. Chem.* **1975**, *14*, 950. (d) Kleier, D. A.; Lipscomb, W. N. *Inorg. Chem.* **1979**, *18*, 1312.

(2) (a) Guggenberger, L. J.; Muetterties, E. L. *J. Am. Chem. Soc.* **1976**, *98*, 7221. (b) Klanberg, F.; Muetterties, E. L. *Inorg. Chem.* **1966**, *5*, 1955. (c) Lipscomb, W. N. *Science* **1966**, *153*, 173. (d) Tolpin, E. I.; Lipscomb, W. N. *J. Am. Chem. Soc.* **1973**, *95*, 2384. (e) Kleier, D. A.; Dixon, D. A.; Lipscomb, W. N. *Inorg. Chem.* **1978**, *17*, 166. (f) Dixon, D. A.; Kleier, D. A.; Halgren, T. A. *J. Am. Chem. Soc.* **1977**, *99*, 6226.

(3) (a) Wales, D. J.; Stone, A. J. *Inorg. Chem.* **1987**, *26*, 3845. (b) Wales, D. J.; Mingos, D. M. P.; Zhenyang, L. *Inorg. Chem.* **1989**, *28*, 2754. (c) Mingos, D. M. P.; Wales, D. J. In *Electron Deficient Boron and Carbon Clusters*; Olah, G. A., Wade, K., Williams, R. E., Eds.; Wiley: New York, 1991; Chapter 5, p 143. (d) Wales, D. J.; Bone, G. A. *J. Am. Chem. Soc.* **1992**, *114*, 5399.

(4) (a) King, R. B. *Inorg. Chim. Acta* **1981**, *49*, 237. (b) Gimarc, B. M.; Ott, J. J. *Inorg. Chem.* **1986**, *25*, 2708. (c) Ott, J. J.; Brown, C. A.; Gimarc, B. M. *Inorg. Chem.* **1989**, *28*, 4269. (d) Gimarc, B. M.; Ott, J. J. *Main Group Met. Chem.* **1989**, *12*, 77. (e) Gimarc, B. M.; Daj, B.; Warren, D. S.; Ott, J. J. *J. Am. Chem. Soc.* **1990**, *112*, 2597.

(5) (a) Gaines, D. F.; Coons, D. E.; Heppert, J. A. In *Advances in Boron and Boranes*; Liebmann, F. F., Greenberg, A., Williams, R. E., Eds.; VCH Publishers: Weinheim, New York, 1988; Chapter 5, p 91. (b) Edvenson, G. M.; Gaines, D. F. *Inorg. Chem.* **1990**, *29*, 1210.

(6) (a) Groszek, E.; Leach, J. B.; Wong, J. T. F.; Ungermann, C.; Onak, T. *Inorg. Chem.* **1971**, *10*, 2770. (b) McKee, M. L. *J. Phys. Chem.* **1989**, *93*, 3426. (c) Mebel, A. M.; Charkin, O. P. *Russ. J. Inorg. Chem.* (*Engl. Transl.*) **1990**, *35*, 174.

(7) (a) Wegner, P. A.; Adams, D. M.; Callabretta, F. J.; Spada, L. T.; Unger R. G. *J. Am. Chem. Soc.* **1973**, *22*, 7513. (b) Vinitskii, D. M.; Lagun, V. L.; Solntsev, K. A.; Kuznetsov, N. T.; Kuznetsov, I. Yu. *Koord. Khim.* **1985**, *11*, 1504 (in Russian). (c) Privalov, V. I.; Tarasov, V. P.; Meladze, M. A.; Vinitskii, D. M.; Solntsev, K. A.; Buslaev, Yu. A.; Kuznetsov N. T. *Russ. J. Inorg. Chem.* (*Engl. Transl.*) **1986**, *31*, 633. (d) Mustyatsa, V. N.; Votinova, N. A.; Solntsev, K. A.; Kuznetsov, N. T. *Dokl. Chem. Proc. Sov. Acad. Sci.* (*Engl. Transl.*) **1988**, *301*, 245. (e) Preetz, W.; Heinrich, A.; Thesing, J. *Z Naturforschung.* **1988**, *43B*, 1319. (f) Baurmeister, J.; Franken, A.; Preetz, W. *Z Naturforschung.* **1995**, *50B*, 623.

(8) Kuznetsov, N. T.; Solntsev, K. A. In *Chemistry of Inorganic Hydrides*; Kuznetsov, N. T., Ed.; Nauka Publ.: Moscow, 1990; p 5 (in Russian).

S0020-1669(97)00940-3 CCC: $15.00
Published on Web 04/01/1998

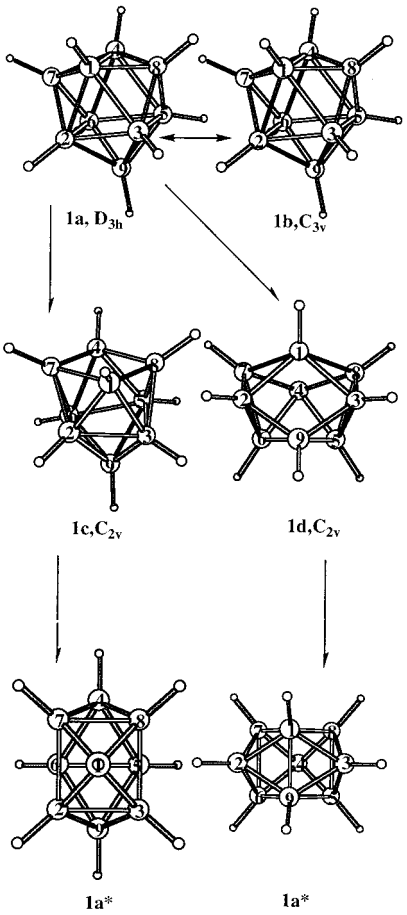

Figure 1. B3LYP/6-311+G** optimized geometries for $B_9H_9^{2-}$ (**1a**−**d**): single and double DSD mechanisms of the **1a** → **1a*** rearrangement.

protonation of $B_9H_9^{2-}$.[8] However, in contrast to salts of the two other well documented $B_nH_{n+1}^-$ anions (n = 6, 10), the $[Ni(Bipy)_3](B_9H_{10})_2$ and $[Ni(Phen)_3](B_9H_{10})$ derivatives of **2** are not stable, and their X-ray analyses could not be carried out.

The NMR ^{11}B spectra of **2** in solution are complicated by the presence of numerous decomposition products (e.g., boric acid and its salts, $B_{12}H_{12}^{2-}$, $B_{10}H_{10}^{2-}$, $B_8H_8^{2-}$, and $B_3H_8^-$). However, three ^{11}B signals of approximately equal intensity were assigned to the $B_9H_{10}^-$ anion.[8] The spectral pattern did not change when the temperature was decreased to −60 °C. These results suggested a trigonal tricapped prism structure (see **2c**, C_{3v}, in Figure 2), where the additional hydrogen atom (designated H*) was thought to be coordinated to a triangular BBB face forming a four-center bonding arrangement akin to that in $B_6H_7^-$.[7b,9a,10a]

In contrast to $B_6H_7^-$, $B_8H_9^-$, and $B_{10}H_{11}^-$, where earlier nonempirical calculations[9,10] agree with the experimental data

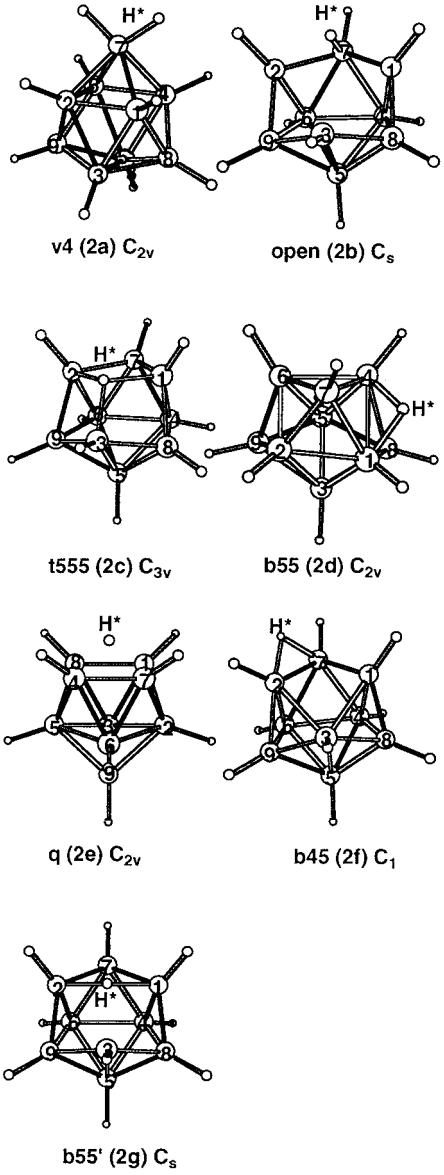

Figure 2. B3LYP/6-311+G** optimized geometries for $B_9H_{10}^-$ (**2a**−**f**).

and conclusions, the previous calculations of $B_9H_{10}^-$ at the STO-3G//MNDO and LP-3lG//MNDO levels[11] (i.e., ab initio SCF single points using the MNDO geometry) did not support the **2c** structure.[8] Instead, v4 (**2a**) (Figure 2), containing a BH_2 group at the capping position, was suggested to be the most stable $B_9H_{10}^-$ form. Several other higher energy alternatives were described: e.g., **2b** with the extra hydrogen H* above a hexagonal nonplanar face of the open boron skeleton (relative energy (RE) = 9 kcal/mol) and t455 with H* over the $B_1B_4B_7$ face (RE = 17 kcal/mol).[11] In contrast, **2c**, the earlier structural candidate,[8] was calculated to be 21 kcal/mol less stable than **2a**.[11]

Although the geometries for $B_6H_7^-$, $B_7H_8^-$, $B_8H_9^-$, and $B_{10}H_{11}^-$ [9,10] did not change significantly when the basis set was expanded from 3-21G to 6-3lG* and the energy ordering remained the same when electron correlation was included (single point computations at the MP2/6-31G* level),[10] quantitative differences in relative energies were found. The present paper reexamines and refines the previous investigation[11] of

(9) (a) Mebel, A. M.; Charkin, O. P.; Kuznetsov, I. Yu.; Solntsev, K. A.; Kuznetsov, N. T. *Russ. J. Inorg. Chem.* (*Engl. Transl.*) **1988**, *33*, 958. (b) Mebel, A. M.; Charkin, O. P.; Solntsev, K. A.; Kuznetsov, N. T. *Russ. J. Inorg. Chem.* (*Engl. Transl.*) **1988**, *33*, 1292; **1989**, *34*, 813. (c) Mebel, A. M.; Charkin, O. P.; Solntsev, K. A.; Kuznetsov, N. T. In *Chemistry of Inorganic Hydrides*; Kuznetsov, N. T., Ed.; Nauka Publ.: Moscow, 1990; p 43 (in Russian). (d) Mebel, A. M.; Charkin, O. P.; Solntsev, K. A.; Kuznetsov, N. T. *Russ. J. Inorg. Chem.* (*Engl. Transl.*) **1989**, *34*, 156.

(10) (a) McKee, M. L.; Bühl, M.; Charkin, O. P.; Schleyer, P. v. R. *Inorg. Chem.* **1993**, *32*, 4549. (b) Bühl, M.; Mebel, A. M.; Charkin, O. P.; Schleyer, P. v. R. *Inorg. Chem.* **1992**, *31*, 3769. (c) Mebel, A. M.; Charkin, O. P.; Bühl, M.; Schleyer, P. v. R. *Inorg. Chem.* **1993**, *32*, 463. (d) Mebel, A. M.; Charkin, O. P.; Schleyer, P. v. R. *Inorg. Chem.* **1993**, *32*, 469.

(11) Mebel, A. M.; Charkin, O. P.; Solntsev, K. A.; Kuznetsov, N. T. *Russ. J. Inorg. Chem.* (*Engl. Transl.*) **1989**, *34*, 808.

$B_9H_{10}^-$ at higher computational levels. Moreover, IGLO[12] chemical shift calculations provide additional information. The combined ab initio/IGLO/NMR method has been applied successfully to the structural elucidation of electron deficient boron compounds,[13,14] carbocations,[15] and protonated *closo*-boranes.[10] Finally, we examine additional members of the $B_nH_{n+1}^-$ set (n = 6−10 and 12) at the same higher levels of theory and draw generalizations concerning their stabilities and proton affinities.

Methods

The geometries were fully optimized[16,17] with the Gaussian-94 program,[17] at the correlated MP2(fc)/6-31G* level using the frozen core approximation (notation MP2(fc)/6-31G*//MP2(fc)/6-31G*), as well as with density functional theory (DFT) at B3LYP/6-31G* and B3LYP/6-311+G**.[17,18] The nature of each stationary point was probed by B3LYP/6-31G*[19] analytical frequency calculations; transition structures have one and minima have zero imaginary frequencies. Zero point energies were scaled by 0.98.[20] Chemical shifts were calculated using the IGLO (individual gauge for localized orbitals) method[12] and GIAO B3LYP/6-311+G**.[21] A DZ Huzinaga basis[22] set was used which was contracted as follows: B 7s3p [4111,21], H 3s [21].

The $B_9H_9^{2-}$ Dianion (1)

In accord with previous conclusions,[2,4] the best $B_9H_9^{2-}$ structure is a tricapped trigonal prism (**1a**) with D_{3h} symmetry (Figure 1). The B3LYP/6-311+G** optimized geometry is in reasonable agreement with experiment (B_1B_2 = 1.93, B_1B_4 = 1.81, B_1B_7 = 1.71 Å).[23] The optimized B_lB_4 bond length (see Figure 1) is within 0.02 Å of the experimental values, while B_lB_2 shows a larger deviation (0.06 Å). At HF/3-21G, a small imaginary frequency (138i cm^{-1}) was calculated for **1a**. However, the C_{3v} minimum at that level (**1b**) proved to be an artifact. When **1b** was optimized at MP2/6-31G*, at B3LYP/6-31G*, and at B3LYP/6-311+G**, **1a** results.

Structure **1c** (C_{2v} symmetry, Figure 1) is the transition state for the degenerate rearrangement of **1a** by the single DSD mechanism in which the B_lB_4 bond is broken in forming the rectangular $B_lB_7B_4B_8$ face. The B_lB_7 and B_4B_7 bonds lengthen to 1.972 Å (B3LYP/6-311+G**), while the B_lB_8 and B_4B_8 bonds shorten to 1.628 Å. Although "symmetry forbidden",[4] transition state **1c** is only 28.4 kcal/mol higher in energy than **1a**.

However, **1d** is the more favorable C_{2v} transition structure for the double DSD rearrangement. Two B_lB_4 and B_2B_3 bonds are broken in **1d** as compared with **1a**, and two rectangular $B_lB_2B_9B_3$ and $B_lB_7B_4B_8$ faces are formed. The activation barrier, 21.3 kcal/mol (B3LYP/6-311+G**), is lower than that for **1c** but still more than sufficiently high to inhibit fluxional behavior on the NMR time scale at room temperature. Thus, our calculations confirm previous experimental and theoretical conclusions:[4] $B_9H_9^{2-}$ is relatively rigid and prefers to rearrange by a double rather than a single DSD mechanisms.

The $B_9H_{10}^-$ Monoanion (2)

The initial trial $B_9H_{10}^-$ geometries of **2** involved the H* atom coordinated to various faces, edges, and vertexes of the parent $B_9H_9^{2-}$ (**1**) structures. Optimization of these initial configurations led to seven stationary points on the $B_9H_{10}^-$ anion PES, **2a**−**g** (Figure 2). The absolute and relative energies are summarized in Table 1.

Although the C_{2v} structure (v4, **2a**) is computed to be the global $B_9H_{10}^-$ minimum at MP2/6-31G* (as was found earlier),[11] **2b** was 1.13 kcal/mol lower in energy at B3LYP/6-311+G**. The energy of third minimum, t555 **2c** (C_{3v} symmetry), was less than 10 kcal/mol higher than **2b**. The geometries of **2a**, which has a BH_2 group at the capping position (B_7), and of **2b** are unusual. $B_9H_{10}^-$ is the first *closo*-borane $B_nH_{n+1}^-$ monoanion where a structure with a BH_2 group is a local minimum. In $B_6H_7^-$, $B_8H_9^-$, and $B_{10}H_{11}^-$, structures with BH_2 groups were transition states for degenerate H* exchange.[9,10] The BH_2-group orientation in **2a** is parallel with the basal planes and extends significantly away from the rest of the boron skeleton. Compared with the corresponding distances in **Ia,** the B_lB_7, B_2B_7, B_4B_7, and B_6B_7 separations are ca. 0.12 Å longer in **2a**. The B_lB_4 and B_2B_6 bonds are elongated even more significantly, 0.19 to 1.98 Å, while the B_lB_2 (B_4B_6) and B_lB_3 (B_2B_3, B_4B_5, B_5B_6) bonds in the prism bases are shortened by 0.20 and 0.10 Å, respectively. Similarly large deformations of the boron skeletons were found for the other $B_7H_8^-$, $B_8H_9^-$, and $B_{10}H_{11}^-$ anion structures containing BH_2 groups.[9,10]

The extra H* in **2b** is located above the open face of $B_9H_9^{2-}$, forming a nonsymmetrical cap with one four-coordinated (B_7) and two three-coordinated (B_1 and B_2) borons (the distances are 1.30 and 1.54 Å). Structure **2b** is related to **2a** via a 90° BH_2 rotation. Although the energy change is small, this rotation results in a remarkable deformation of the boron cage. In particular, the face opens and the B_lB_2 and B_lB_3 bonds and the B_2B_3 bond are elongated to 2.69 and 2.35 Å, respectively.

(12) (a) Kutzelnigg, W. *Isr. J. Chem.* **1980**, *19*, 193. (b) Schindler, M.; Kutzelnigg, W. *J. Chem. Phys.* **1982**, *76*, 1919. Review: (c) Kutzelnigg, W.; Fleischer, U.; Schindler, M. *NMR, Basic Principles and Progress*; Springer-Verlag: Berlin, 1990; p 165.
(13) (a) Schleyer, P. v. R.; Bühl, M.; Fleischer, U.; Koch, W. *Inorg. Chem.* **1990**, *29*, 153. (b) Bühl, M.; Schleyer, P. v. R. *Angew. Chem., Int. Ed. Engl.* **1990**, *29*, 886. (c) Bühl, M.; Schleyer, P. v. R. In *Electron Deficient Boron and Carbon Clusters*; Olah, G. A., Wade, K., Williams, R. E., Eds.; Wiley: New York, 1990; Chapter 4, p 113. (d) Bühl, M.; Schleyer, P. v. R.; McKee, M. L. *Heteroatom Chem.* **1991**, *2*, 499.
(14) Bühl, M.; Schleyer, P. v. R. *J. Am. Chem. Soc.* **1992**, *114*, 477.
(15) (a) Schindler, M. *J. Am. Chem. Soc.* **1987**, *109*, 1020. (b) Bremer, M.; Schleyer, P. v. R.; Schötz, K.; Kausch, M.; Schindler, M. *Angew. Chem.* **1987**, *99*, 795. (c) Schleyer, P. v. R.; Laidig, K. E.; Wiberg, K. B.; Saunders: M.; Schindler, M. *J. Am. Chem. Soc.* **1988**, *110*, 300. (d) Saunders: M.; Laidig, K. E.; Wiberg, K. B.Schleyer, P. v. R. *J. Am. Chem. Soc.* **1988**, *110*, 7652. (e) Schleyer, P. v. R.; Carneiro, J. W. de M.; Koch, W.; Raghavachari, K. *J. Am. Chem. Soc.* **1989**, *111*, 5475. (f) Bremer, M.; Schleyer, P. v. R.; Fleischer, U. *J. Am. Chem. Soc.* **1989**, *111*, 1147. (g) Bremer, M.; Schötz, K.; Schleyer, P. v. R.; Fleischer, U.; Schindler, M.; Kutzelnigg, W.; Pulay, P. *Angew. Chem.* **1989**, *101*, 1063. (h) Schleyer, P. v. R.; Koch, W.; Liu, B.; Fleischer, U. *J. Chem. Soc., Chem. Commun.* **1989**, 1098. (i) Schleyer, P. v. R.; Carneiro, J. W. d. M. *J. Am. Chem. Soc.* **1990**, *112*, 4046.
(16) Hehre, W.; Radom, L.; Schleyer, P. v. R.; Pople, J. A. *Ab Initio Molecular Orbital Theory*; Wiley: New York, 1986.
(17) (a) Frisch, M. J.; Trucks, G. W.; Schlegel, H. B.; Gill, P. M. W.; Johnson, B. G.; Robb, M. A.; Cheeseman, J. R.; Keith, T.; Petersson, G. A.; Montgomery, J. A.; Raghavachari, K.; Al-Laham, M. A.; Zakrzewski, V. G.; Ortiz, J. V.; Foresman, J. B.; Cioslowski, J.; Stefanov, B. B.; Nanayakkara, A.; Challacombe, M.; Peng, C. Y.; Ayala, P. Y.; Chen, W.; Wong, M. W.; Andres, J. L.; Replogle, E. S.; Gomperts, R.; Martin, R. L.; Fox, D. J.; Binkley, J. S.; Defrees, D. J.; Baker, J.; Stewart, J. P.; Head-Gordon, M.; Gonzalez, C.; Pople, J. A. *Gaussian 94*, Revision C.3; Gaussian Inc.: Pittsburgh, PA, 1995. (b) Foresman, J. B.; Frisch, A. *Exploring Chemistry with Electronic Structure Methods*, 2nd ed., Gaussian, Inc.: Pittsburgh, PA, 1995−1996.
(18) (a) Becke, A. D. *J. Chem. Phys.* **1993**, *98*, 5648. (b) Lee, C.; Yang, W.; Parr, R. G. *Phys. Rev. B* **1988**, *37*, 785.
(19) Scott, A. P.; Radom, L. *J. Phys. Chem.* **1996**, *100*, 16502 and references therein.
(20) Bauschlicher, C. W., Jr.; Partridge, H. *J. Chem. Phys.* **1995**, *103*, 1788.
(21) Wolinksi, K.; Hinton, J. F.; Pulay, P. *J. Am. Chem. Soc.* **1990**, *112*, 8251.
(22) Huzinaga, S. *Approximate Atomic Wave Functions*, University of Alberta: Edmonton, Canada, 1971.
(23) Guggenberger, L. J. *Inorg. Chem.* **1968**, *7*, 2260.

Table 1. Absolute (−au) and Relative Energies (kcal/mol) for Different $B_9H_9^{2-}$ and $B_9H_{10}^-$ Structures

struct sym	no.	level B3LYP/6-31G*	ZPE[a] (NIMAG)	level MP2/6-31G*	rel energies[b]	level B3LYP/6-311+G**	rel energies[b]
				$B_9H_9^{2-}$			
D_{3h}[c]	**1a**	229.12195	74.45 (0)	228.16066	0.00	229.19051	0.00
C_{2v}	**1c**	229.07277	73.16 (1)	228.10540	33.41	229.14329	28.36
C_{2v}	**1d**	229.08469	73.56 (1)	228.11967	24.84	229.15523	21.25
				$B_9H_{10}^-$			
v4, C_{2v}	**2a**	229.79516	81.79 (0)	228.82269	0.00	229.84573	0.00
open, C_s	**2b**	229.79329	81.50 (0)	228.81747	3.00	229.84708	−1.13
t555, C_{3v}	**2c**	229.77491	80.47 (0)	228.79677	14.97	229.82992	8.63
b55, C_{2v}	**2d**	229.75265	80.33 (1)	228.77956	25.63	229.80806	22.21
q, C_{2v}	**2e**	229.74924	78.97 (1)	228.77411	27.72	229.80393	23.46
b45, C_1	**2f**	229.78007	81.62 (1)	228.80618	10.19	229.83365	7.41
b55′, C_s	**2g**	229.77323	79.75 (1)	228.79542	15.11	229.82850	8.81

[a] Zero-point energy (kcal/mol), calculated at B3LYP/6-31G(d). In parentheses: number of imaginary frequencies, NIMAG. [b] The relative energies with ZPE corrections scaled by 0.98 in kcal/mol. [a]A C_{3v} minimum, found at lower levels of theory, optimizes to D_{3h} when electron correlations are included.

Like $B_8H_9^-$,[10b] protonation of $B_9H_9^{2-}$ results in opening of the boron skeleton and transformation of the *closo*- into a *nido*-form. But unlike $B_8H_9^-$, where the energies of the "open" configurations were significantly above that of the global minimum, **2b** for $B_9H_{10}^-$ has almost the same energy as the "closed" **2a** structure. A C_{3v} minimum (**2c**, t555) is 8.7 kcal/mol higher in energy than **2a** at B3LYP/6-311+G**. The additional H* in **2c** is situated above an open BBB face of **1a** forming a symmetrical four-center cap with the B_1, B_2, and B_3 atoms. Protonation of **1a** elongates the B_1B_2, B_1B_3, and B_2B_3 distances by 0.32 Å in **2e**. The t455 structure with H* over the $B_1B_4B_7$ face, assumed to be a minimum at the LP-3lG//MNDO level,[11] is not a stationary point and transforms into **2a** without barrier upon optimization.

Nonrigid Behavior. According to our calculations, $B_9H_{10}^-$ should have a relatively rigid boron skeleton (like $B_9H_9^{2-}$). Configuration **2d** (C_{2v}, b55), a transition structure for the degenerate **2a** → **2a*** rearrangement (H* migration from one capping boron to another), has one imaginary frequency at B3LYP/6-31G* and lies 22.2 kcal/mol (B3LYP/6-311+G**) higher than **2a**. We found also a different C_{2v} form (**2e**) in which symmetry planes are rotated by 45°, with respect to **2d**. No B_1B_4 bond is present in **2e**, and the extra H* hydrogen is coordinated symmetrically above the center of the rectangular $B_1B_7B_4B_8$ face. Similar transition states with five-center bonds between the capping H* and the boron skeleton were found earlier for $B_8H_9^-$.[10b] With one imaginary frequency, structure **2e** is 1.3 kcal/mol higher in energy than **2d** at B3LYP/6-311+G**. Both configurations help delineate different degenerate **2a** → **2a*** rearrangement pathways: **2d** corresponds to the H* migration which scrambles all capping B_7-B_9 and all basal B_1-B_6 atoms, while **2e** is related with a more complicated concerted H* migration, coupled with cage reconstruction. However, the processes, 22.2 and 23.6 kcal/mol via **2d** and **2e**, may be too high in energy to allow rearrangement at the lower temperatures where $B_9H_{10}^-$ can exist in solution.

This capped antiprism structure is stabilized by protonation: **2e** is higher than **2a** by 23.5 kcal/mol, while **1c** is less stable than **1a** by 28.4 kcal/mol (B3LYP/6-311+G**). The B_4B_7 and B_1B_7 bond lengths of the bridged tetragonal face change most from **1c** and are elongated in **2e** by 0.5 and 0.20 Å, respectively.

Isomer **2b** with the open boron skeleton should be fluxional. The external hydrogen H* can migrate from B_7 to B_8 or to B_9 via the center of the hexagonal face. The rearrangement occurs by the **2b** → TS **2g** → **2c** → TS **2g*** → **2b*** mechanism: Structure **2g** (C_s), where H* is located above the B_1B_2 edge, serves as the transition state. At the B3LYP/6-311+G** level, the barriers are 9.9 and 0.2 kcal/mol with respect to **2b** and the very shallow minimum, **2c**, respectively. We failed to find another **2b** → **2b*** migration pathway with an activation energy lower than 9.9 kcal/mol. Candidate structures containing a BH_2 group, both nonsymmetrical and symmetrical, transformed into **2c** when optimized in C_s symmetry.

The search for the transition state between **2a** and **2b** led to structure **2f**, which has no symmetry and the additional hydrogen located over the B_1B_7 edge. The **2a** → **2b** scrambling involves twisting the BH_2 group by 90°. The calculated barriers involving transition state **2f** are 7.4 and 8.5 kcal/mol relative to **2a** and **2b**, respectively, at B3LYP/6-311+G**. Therefore, the **2a** → **2b** isomerization should be facile at ambient temperatures.

The feasible rearrangements of $B_9H_{10}^-$ are summarized as follows:

2b → TS **2g** → **2c** → TS **2g*** → **2b*** (1)

2b → TS **2f** → **2a** → TS **2f*** → **2b*** (2)

2a → TS **2d** → **2a*** (3)

2a → TS **2e** → **2a*** (4)

In process 1, H* scrambles around one of the triangle prism bases ($B_1-B_2-B_3$) via its center. In (2), the extra hydrogen migrates from one prism base to another ($B_4-B_5-B_6$). The two processes combined result in the migration of H* around the whole boron skeleton: **2b** → TS **2g** → **2c** → TS **2g*** → **2b*** → TS **2f** → **2a** → TS **2f*** → **2b****, etc. The barriers on this pathway are 8.5 and 9.9 kcal/mol. Hence, at ambient temperature, the NMR spectra should show equivalent the B_1-B_6 and B_7-B_9 boron atoms. The barriers involving the transition states **2d** and **2e** are much higher. Thus, the prism edges, B_1-B_4, B_2-B_6, and B_3-B_5, should be avoided by H* in favor of other routes.

Electronic Structure

Interatomic distances and natural atomic charges and Wiberg bond indices (WBI)[24] obtained from the natural population analysis[25] are summarized in Table 3. In the parent $B_9H_9^{2-}$ **1a** structure, the four-coordinated capping B_7-B_9 atoms have the largest negative charges (−0.347 e). These should be preferred centers for electrophilic attack. Indeed, in the $B_9H_{10}^-$ **2a**,**b** structures, the additional hydrogen is bonded to the capping

(24) Wiberg, K. B. *Tetrahedron* **1968**, *24*, 1083.
(25) Reed, A. E.; Curtiss, L. A.; Weinhold, F. *Chem. Rev.* **1988**, *88*, 899.

Table 2. Selected Interatomic Distances (Å) for $B_9H_9^{2-}$ and $B_9H_{10}^-$ at the B3LYP/6-311+G** Level, with the Atom Numbering Shown in Figures 1 and 2

	D_{3h} (**1a**)	C_{2v} (**1c**)	C_{2v} (**1d**)	v4, C_{2v} (**2a**)	open, C_s (**2b**)	t555, C_{3v} (**2c**)	b55, C_{2v} (**2d**)	q, C_{2v} (**2e**)	b55′, C_s (**2g**)	b45, C_1 (**2f**)
B1B2	1.992	1.760	1.862	1.789	2.686	2.312	1.911	1.796	2.501	2.315
B2B3		1.897	2.793	1.889	2.348		2.052	1.888	2.285	2.064
B1B3		1.833						1.760		2.096
B1B4	1.789	2.557	2.254	1.978	1.749	1.757	2.046	2.698	1.749	1.782
B2B6			1.759				1.768			1.859
B3B5				1.799	1.812				1.780	1.815
B4B5			1.825		1.833	1.885			1.874	1.826
B5B6			1.845							1.878
B4B6					1.847				1.868	1.854
B1B7	1.712	1.972	1.862	1.830	1.806	1.738	1.821	1.686	1.786	1.748
B2B7			1.605				1.681			1.768
B4B7		1.628	1.731		1.762	1.727		2.106	1.725	1.758
B1B8				1.703	1.650				1.686	1.639
B3B8				1.719	1.696					1.709
B4B8					1.754	1.727			1.741	1.749
B5B8					1.745				1.732	1.724
B2B9		1.837				1.738	1.714	1.644		1.705
B3B9		1.646								1.704
BH*				1.200	1.299	1.474	1.336	1.532	1.434	1.280
					1.536					1.300

Table 3. Selected Wiberg Bond Indices and Natural Charges for $B_9H_9^{2-}$ and $B_9H_{10}^-$ at the B3LYP/6-311+G** Level, with the Atom Numbering Shown in Figures 1 and 2

Wiberg Bond Indices

	D_{3h} (**1a**)	C_{2v} (**1c**)	C_{2v} (**1d**)	v4, C_{2v} (**2a**)	open, C_s (**2b**)	t555, C_{3v} (**2c**)	b55, C_{2v} (**2d**)	q, C_{2v} (**2e**)	b55′, C_s (**2g**)
B1B2	0.411	0.674	0.515	0.588	0.084	0.20	0.445	0.492	0.130
B2B3		0.458	0.027	0.443	0.264		0.331	0.453	0.233
B1B3		0.475						0.673	
B1B4	0.495	0.124	0.253	0.370	0.536	0.504	0.319	0.045	0.520
B2B6			0.553				0.487		
B3B5				0.501	0.445				0.479
B4B5			0.519		0.501	0.440			0.460
B5B6			0.540						
B4B6					0.486				0.466
B1B7	0.678	0.349		0.502	0.545	0.666	0.548	0.813	0.601
B2B7			0.903				0.701		
B4B7		0.999	0.691		0.577	0.634		0.303	0.634
B1B8				0.676	0.823	0.666			0.744
B3B8				0.633	0.751				
B4B8					0.573				0.602
B5B8					0.607				0.631
B2B9		0.454				0.666	0.658		
B3B9		0.834						0.040	
BH*				0.812	0.469	0.287	0.342	0.224	0.315
					0.956				

Natural Charges

	D_{3h} (**1a**)	C_{2v} (**1c**)	C_{2v} (**1d**)	v4, C_{2v} (**2a**)	open, C_s (**2b**)	t555, C_{3v} (**2c**)	b55, C_{2v} (**2d**)	q, C_{2v} (**2e**)	b55′, C_s (**2g**)
B1	−0.129	−0.176	+0.070	−0.048	+0.080	−0.037	−0.177	−0.089	−0.686
B2		−0.210	−0.292				−0.127	−0.235	
B3		−0.198		−0.162	+0.116			−0.198	+0.555
B4	−0.129		−0.161		−0.175	−0.164			−0.185
B5			−0.174		−0.146				−0.150
B6									
B7	−0.347			−0.431	−0.296	−0.251	−0.188		−0.133
B8					−0.415				−0.312
B9		−0.241		−0.228			−0.289	−0.143	
H*				+0.141	+0.184	+0.152	+0.298	+0.215	+0.165

boron atom. In accord with a simple electrostatic model, **2b** is favored over **2c**.

As in other *closo*-boranes dianions, protonation of $B_9H_9^{2-}$ results in charge reduction and the formation of a new BH bond. Consequently, electron density redistribution occurs over the cage. The largest negative charges remain on the boron atoms coordinated to four other borons, both protonated (B_7 in **2a**, −0.431 e) and nonprotonated (B_8 and B_9 in **2b**, −0.415 e). In **2a**, the B_1, B_2, B_4, and B_6 atoms, adjacent to the BH_2 group, have the smallest charges. The B_3 atom in **2b**, located opposite to H* in the hexagonal face, is positively charged (+0.116 e). The WBI[24] (Wiberg bond index) values (see Table 3) correlate qualitatively with the trends in BB and BH bond lengths.

IR Frequencies. The differences in the IR spectra of $B_9H_9^{2-}$ and $B_9H_{10}^-$ are significant (see Tables 4 and 5). The terminal BH stretching vibrations shift to higher wavenumbers (by 60−150 and 110−170 cm^{-1} for $B_9H_{10}^-$ **2a**,**b**, respectively, as compared with **1a**). The similar trends, observed for $B_6H_7^-$

Table 4. IR Wavenumbers (cm^{-1}) and Intensities (kM/mol, in Brackets) for $B_9H_9^{2-}$, Calculated at the B3LYP/6-31G(d) Level

1a (D_{3h})		**1c** (C_{2v})		**1d** (C_{2v}')		**1a** (D_{3h})		**1c** (C_{2v})		**1d** (C_{2v}')	
a_2''	188 [0.0]	a_2	414i	b_2	365i	a_2'	1011 [0.0]	b_2	860 [2]	a_1	868 [8]
e''	144 [0.0]	a_2	261 [0.0]	a_1	286 [0.1]	e'	1084 [29]	a_2	872 [0.0]	b_2	883 [1]
e'	441 [0.0]	b_1	393 [1]	a_2	318 [0.0]	e''	2455 [0.0]	a_2	881 [0.0]	b_1	884 [2]
a_1'	542 [0.7]	b_2	410 [0.5]	a_1	422 [1]	e'	2467 [252]	b_2	895 [1]	b_2	906 [0.3]
a_1''	562 [0.0]	a_1	500 [0.1]	b_2	485 [1]	a_2''	2469 [1043]	b_1	899 [1]	b_1	906 [0.9]
e'	592 [0.4]	a_1	519 [2]	b_1	534 [0.1]	a_1'	2472 [0.0]	a_2	912 [0.0]	a_2	907 [0.0]
a_2''	649 [2]	b_2	531 [0.7]	a_2	588 [0.0]	e'	2499 [796]	a_1	918 [0.3]	a_1	934 [0.1]
e''	668 [0.0]	b_1	539 [1]	b_2	585 [0.6]	a_1'	2528 [0.0]	b_1	920 [9]	a_2	943 [0.0]
a_2'	708 [0.3]	a_2	560 [0.0]	a_1	593 [6]			b_2	931 [5]	b_1	977 [11]
e'	729 [3]	b_1	588 [0.1]	a_2	596 [0.0]			a_2	940 [0.0]	a_1	979 [18]
e''	760 [0.0]	b_2	594 [2]	a_1	657 [0.9]			a_1	1018 [0.2]	a_2	993 [0.0]
a_1'	767 [0.0]	a_1	608 [0.0]	b_1	683 [0.8]			b_2	1019 [11]	b_1	1001 [1]
e'	784 [0.8]	a_1	655 [0.2]	b_2	683 [0.4]			b_1	1014 [6]	b_2	1016 [2]
a_1'	795 [0.0]	b_2	659 [1]	b_1	691 [5]			b_1	1093 [25]	a_1	1124 [5]
e''	855 [0.0]	a_2	671 [0.0]	a_1	697 [0.8]			a_1	1100 [14]	b_1	1152 [78]
a_2''	876 [5]	b_1	695 [6]	b_1	710 [2]			a_2	245 [0.0]	a_1	2407 [391]
a_1'	896 [0.0]	b_2	730 [2]	b_2	719 [5]			b_2	2456 [103]	b_2	2420 [545]
a_1''	896 [0.0]	a_1	751 [1]	a_2	722 [0.0]			a_1	2460 [23]	a_1	2420 [0.3]
e''	896 [0.0]	b_1	791 [1]	a_1	777 [3]			b_1	2461 [2]	b_1	2455 [60]
e'	898 [5]	b_1	801 [20]	b_1	786 [6]			a_1	2467 [291]	a_1	2470 [766]
a_2'	922 [0.0]	a_1	823 [0.3]	b_2	786 [0.0]			b_1	2476 [1060]	a_2	2480 [0.0]
e''	928 [0.0]	a_1	832 [2]	a_1	808 [0.1]			b_2	2480 [1111]	b_2	2483 [669]
e'	996 [2]	b_2	838 [2]	b_2	827 [14]			a_1	2469 [553]	b_1	2498 [855]
a_2''	1006 [26]	a_1	857 [1]	a_2	849 [0.0]			a_1	2524 [870]	a_1	2520 [6]

Table 5. IR Wavenumbers (cm^{-1}) and Intensities (kM/mol, in Brackets) for $B_9H_{10}^-$, Calculated at the B3LYP/6-31G(d) Level

v4, C_{2v} (**2a**)		open, C_s (**2b**)		t555, C_{3v} (**2c**)		b55, C_{2v} (**2d**)		q, C_{2v} (**2e**)		b45, C_1 (**2f**)		b55′, C_s (**2g**)	
b_2	287 [17]	a''	254 [0.0]	e	240 [5]	b_1	1061i	b_2	866i		371i	a'	571i
b_1	407 [0.1]	a'	283 [0.8]	a_1	343 [0.0]	b_2	263 [0.2]	a_2	148 [0.0]		278 [4]	a'	215 [0.0]
a_2	445 [0.0]	a'	325 [5]	e	454 [0.5]	a_1	309 [0.0]	a_2	324 [0.0]		309 [7]	a''	285 [4]
b_1	455 [4]	a''	378 [15]	a_2	487 [0.0]	a_2	317 [0.0]	b_1	363 [3]		353 [0.1]	a'	366 [2]
b_2	480 [10]	a'	503 [0.4]	a_1	580 [0.6]	b_2	331 [0.1]	b_2	422 [3]		507 [0.8]	a''	474 [0.4]
a_1	485 [0.0]	a''	529 [0.1]	e	585 [0.2]	a_1	430 [0.2]	a_1	497 [0.0]		515 [1]	a'	481 [0.2]
a_2	508 [0.0]	a'	566 [2]	e	616 [0.1]	a_2	475 [0.0]	b_1	506 [0.0]		528 [0.9]	a''	506 [0.1]
a_1	549 [5]	a'	591 [0.9]	a_1	655 [4]	b_1	499 [0.0]	a_1	537 [0.1]		555 [2]	a'	571 [0.8]
b_2	560 [0.5]	a''	599 [0.5]	e	674 [3]	a_1	578 [1]	b_2	560 [0.3]		586 [2]	a'	612 [0.7]
a_1	600 [10]	a''	605 [7]	a_2	711 [0]	b_2	616 [2]	a_2	574 [0.0]		611 [2]	a''	613 [0.0]
b_2	613 [0.0]	a'	640 [1]	e	729 [1]	b_1	626 [0.7]	b_1	589 [2]		645 [0.4]	a'	631 [1]
a_2	627 [0.0]	a''	653 [0.0]	e	750 [0.3]	a_2	640 [0.0]	a_1	631 [0.4]		659 [1]	a''	631 [0.1]
b_1	653 [9]	a'	684 [2]	a_1	760 [0.1]	a_1	650 [0.1]	b_2	641 [6]		669 [2]	a'	659 [3]
a_1	676 [0.5]	a'	698 [3]	a_1	786 [2]	b_2	669 [2]	b_1	653 [0.9]		680 [3]	a''	693 [18]
a_2	679 [0.0]	a''	722 [13]	e	789 [5]	b_1	705 [2]	a_1	664 [0.0]		708 [0.2]	a'	705 [1]
a_1	708 [2]	a'	738 [12]	e	841 [21]	b_1	725 [0.5]	a_2	695 [0.0]		718 [3]	a''	716 [2]
b_1	728 [5]	a''	738 [3]	a_2	853 [0.0]	a_2	736 [0.0]	b_2	716 [0.8]		740 [2]	a''	743 [3]
b_1	755 [0.0]	a'	743 [0.5]	a_1	868 [1]	a_1	748 [0.7]	b_1	723 [2]		756 [3]	a'	744 [3]
b_2	765 [0.1]	a'	752 [1]	a_1	900 [0.4]	b_1	754 [3]	a_1	734 [0.9]		771 [1]	a''	759 [4]
a_2	770 [0.0]	a''	768 [3]	e	903 [0.0]	b_2	761 [2]	b_2	757 [12]		775 [1]	a'	760 [0.3]
a_1	773 [2]	a'	790 [1]	e	909 [0.3]	a_1	783 [0.0]	b_2	800 [1]		787 [2]	a'	772 [6]
b_2	805 [3]	a''	793 [0.4]	a_2	924 [0.0]	b_2	796 [0.1]	b_1	804 [5]		793 [6]	a'	779 [2]
a_1	817 [1]	a'	811 [0.2]	e	961 [1]	a_1	797 [4]	a_1	811 [0.4]		829 [0.3]	a''	814 [18]
b_1	832 [4]	a'	841 [10]	a_2	975 [0.0]	a_1	831 [0.0]	a_1	821 [0.0]		857 [2]	a'	820 [3]
a_2	862 [0.0]	a''	848 [4]	a_1	988 [18]	b_2	836 [10]	b_1	832 [0.1]		862 [3]	a''	827 [11]
b_1	877 [0.2]	a'	868 [0.8]	e	1010 [2]	a_2	839 [0.0]	a_1	851 [3]		872 [6]	a''	853 [0.3]
a_1	882 [6]	a'	880 [1]	e	1216 [0.9]	b_1	868 [4]	a_2	857 [0.0]		882 [0.9]	a'	857 [16]
a_1	908 [0.0]	a''	892 [0.0]	a_1	1410 [13]	a_1	876 [0.1]	a_2	865 [0.0]		894 [0.9]	a'	870 [3]
a_2	910 [0.0]	a''	903 [2]	e	2599 [84]	b_2	878 [0.3]	b_1	876 [0.5]		897 [1]	a'	891 [0.0]
b_1	912 [0.3]	a''	918 [0.7]	a_1	2608 [252]	a_2	880 [0.0]	a_1	894 [0.0]		910 [0.1]	a'	904 [2]
b_2	920 [0.7]	a'	921 [0.2]	e	2639 [192]	a_2	893 [0.0]	b_2	896 [0.6]		913 [0.5]	a''	908 [0.0]
a_2	933 [0.0]	a'	932 [0.3]	a_1	2640 [110]	b_2	906 [0.7]	a_2	920 [0.0]		922 [3]	a''	912 [0.0]
b_1	936 [3]	a''	942 [0.0]	e	2655 [232]	b_1	909 [0.4]	a_2	923 [0.0]		926 [2]	a'	924 [0.2]
b_2	940 [0.2]	a''	964 [0.3]	a_1	2669 [72]	a_2	911 [0.0]	b_1	925 [0.9]		938 [0.4]	a''	931 [0.3]
a_1	950 [0.8]	a'	974 [8]			b_1	949 [1]	b_2	928 [13]		943 [1]	a'	957 [5]
b_2	964 [1]	a''	981 [3]			a_1	975 [2]	a_1	956 [2]		980 [12]	a''	967 [0.2]
a_2	969 [0.0]	a''	1020 [9]			b_2	997 [22]	b_2	1008 [0.0]		997 [4]	a''	978 [0.1]
b_1	991 [12]	a'	1025 [2]			b_1	1008 [0.6]	b_1	1037 [12]		1003 [5]	a'	1002 [11]
a_1	1034 [16]	a'	1052 [17]			a_1	1051 [4]	a_1	1047 [0.1]		1037 [6]	a''	1044 [16]
b_2	1056 [0.2]	a'	1127 [1]			b_1	1089 [8]	b_2	1071 [29]		1086 [10]	a'	1047 [5]
a_1	1143 [2]	a''	1135 [4]			b_2	1779 [25]	b_1	1215 [67]		1814 [15]	a'	1387 [11]
a_1	2536 [88]	a'	2012 [5]			a_1	1840 [0.0]	a_1	1509 [1]		2104 [0.3]	a''	1495 [51]
b_2	2548 [43]	a'	2594 [93]			a_2	2605 [0.0]	a_1	2596 [7]		2560 [124]	a'	2594 [109]
b_1	2063 [36]	a''	2602 [11]			b_2	2607 [53]	b_2	2599 [201]		2594 [98]	a'	2601 [71]
a_2	2607 [0.0]	a'	2605 [46]			a_1	2612 [148]	b_1	2606 [227]		2602 [58]	a'	2608 [239]
a_1	2611 [184]	a''	2612 [239]			b_1	2615 [204]	a_1	2610 [67]		2603 [132]	a''	2633 [183]
b_2	2611 [156]	a'	2614 [369]			b_2	2616 [431]	a_2	2638 [0.0]		2606 [118]	a'	2634 [156]
b_1	2619 [489]	a'	2627 [292]			a_1	2621 [18]	b_1	2644 [349]		2613 [311]	a'	2642 [111]
a_1	2622 [131]	a'	2642 [127]			a_1	2643 [249]	b_2	2649 [274]		2619 [270]	a'	2652 [294]
b_2	2639 [151]	a''	2652 [229]			b_1	2672 [259]	a_1	2650 [379]		2636 [333]	a''	2654 [294]
a_1	2652 [49]	a'	2662 [114]			a_1	2677 [59]	a_1	2665 [22]		2650 [93]	a'	2667 [70]

Table 6. ^{11}B Chemical Shifts (ppm) for the $B_9H_9^{2-}$ and the $B_9H_{10}^-$ Anions

	$B_9H_9^{2-}$ **1a**, D_{3h}			$B_9H_9^{2-}$ **1a**, D_{3h}	
level of theory	B(1−6)	B(7−9)	level of theory	B(1−6)	B(7−9)
DZ//3-21G[a]	−15.5	−6.9	HF/6-31+G*//B3LYP/6-311+G**[b]	−19.7	−4.0
DZ//6-31G*[a]	−18.8	−8.9	B3LYP/6-311+G**//B3LYP/6-311+G**[b]	−26.4	−8.7
DZ//MP2/6-31G*[a]	−21.0	−8.4	expt[c]	−21.3	−3.2

	$B_9H_{10}^-$ **2a**, C_{2v}					
level of theory	B(3,5)	B(1,2,4,6)	B(7)	B(8,9)	B(1−6)[e]	B(7−9)[e]
DZ//3-21G[a]	−12.5	+21.3	+16.1	+43.6	(+10.3)	(+34.3)
DZ//6-31G*[a]	−13.8	+19.0	+13.2	+42.5	(+8.1)	(+32.7)
DZ//MP2/6-31G*[a]	−16.1	+14.3	+1.1	+43.2	(+4.1)	(+29.2)
II′//MP2/6-31G*[a]	−18.2	+13.6	+2.9	+45.9	(+3.0)	(+29.6)
HF/6-31+G*//B3LYP/6-311+G**[b]	−12.3	+18.9	+10.5	+47.1	(+8.5)	(+34.9)
B3LYP/6-311+G**// B3LYP/6-311+G**[b]	−24.2	+10.3	−5.7	+40.8	(−1.2)	(+25.3)
expt[d]	+8.9(3B)	+11.3(3B)	+28.3(3B)			

	$B_9H_{10}^-$ **2b**, C_s								
level of theory	B(1,2)	B(3)	B(4,6)	B(5)	B(7)	B(8,9)	B(1−3)[e]	B(4−6)[e]	B(7−9)[e]
DZ//3-21G[a]	+18.4	+29.0	−14.8	−1.7	−17.1	−6.4	(+21.9)	(−6.1)	(−9.8)
HF/6-31+G*//B3LYP/6-311+G**[b]	+11.9	+19.2	−11.6	−5.2	−16.2	+2.6	(+14.3)	(−9.5)	(−3.7)
B3LYP/6-311+G**// B3LYP/6-311+G**[b]	−0.7	+8.4	−19.0	−16.4	−25.6	−0.8	(+2.3)	(−18.2)	(+9.1)

	$B_9H_{10}^-$										
	2c, C_{3v}			**2d**, C_{2v}				**2e**, C_{2v}			
level of theory	B(1−3)	B(4−6)	B(7−9)	B(1−4)	B(2,3,5,6)	B(7,8)	B(9)	B(1,4,7,8)	B(2,5)	B(3,6)	B(9)
DZ//3-21G[a]	−9.6	−2.2	+5.2	−15.2	−15.4	−1.9	−11.1	+4.9	−19.1	−7.8	+22.6

[a] IGLO. [b] GIAO. [c] Data from ref 27. [d] Data from ref 8. [e] Averaged values.

and $B_{10}H_{11}^-$ experimentally[7,8] and for $B_7H_8^-$ and $B_8H_9^-$ theoretically,[9,10] are in accord with the small but systematic shortening of the BH terminal bonds in the monoanions vs the dianions.

Characteristic $B_9H_{10}^-$ IR vibrations are associated with the additional hydrogen, H*. For **2a**, this feature is the BH_2^- group bending mode (computed frequency 1143 cm^{-1}). For **2b**, the characteristic frequency observed at 2012 cm^{-1} corresponds to the stretching vibration of B_7H^* fragment in the nonsymmetric $B_7(H^*)\,B_lB_2$ bond (cf. with 2144 cm^{-1} in $B_{10}H_{11}^-$).[8] In **2c**,**e**, where H* is involved to weak multicenter bonding with three and four boron atoms (with long BH* distances, 1.474 and 1.532 Å), respectively, the characteristic frequencies are 1410 and 1509 cm^{-1} (cf. 1401 cm^{-1} for $B_{10}H_{11}^-$ and 1440−1470 cm^{-1} for $B_8H_9^-$).[10]

The normal three-center bridge B(H*)B bond stretching frequency is 1840 cm^{-1} in **2d**. Each type of bonding between the boron skeleton and the additional hydrogen has a characteristic IR frequency.[26]

Chemical Shift Calculations. The computed chemical shifts for $B_9H_9^{2-}$ and $B_9H_{10}^-$ isomers at various levels are summarized in Table 6. The calculated values agree within 3−5 ppm with experiment for the D_{3h} $B_9H_9^{2-}$ dianion **1a**. The IGLO values for other $B_nH_n^{2-}$ dianions, computed earlier at the same levels of theory,[10,13] reproduced the experimental results with an accuracy of ±3 ppm.

The reported NMR ^{11}B spectrum of $B_9H_{10}^-$ was not refined, but three signals of approximately equal intensity, with chemical shifts +8.9, +11.3, and +28.3 ppm,[8] were assigned to the **2c** structure of $B_9H_{10}^-$.[8] Our calculations cast doubt on this interpretation, because **2c** is a very shallow minimum lying 9.8 kcal/mol higher than **2b**. Moreover, the chemical shifts of **2c**, −9.6 (3B), −2.2 (3B), and +5.2 ppm (3B), calculated at the IGLO level, differ drastically from the experimental values by 13−23 ppm. This is several times larger than the accuracy expected of the IGLO calculations based on the results for related species.[14]

Since the relative stabilities of **2a**,**b** depend on the level of theory (Table 1), both should be compared with experiment. The computed spectrum of **2b** has another pattern and intensity ratio, 1:2:1:2:1:2. Migration of H* among the B_7, B_8, and B_9 atoms via the center of the nonplanar hexagonal face (transition structure **2g**, barrier 9.9 kcal/mol) could scramble the B_l-B_3, B_4-B_6, and B_7-B_9 atoms on the NMR time scale, and three signals of equal intensity would be observed. Nevertheless, this possibility also is excluded as the corresponding GIAO B3LYP/6-311+G** chemical shifts, +2.3, −18.2, and +9.1 ppm, are 11−29 ppm from the experimental values.

The NMR ^{11}B spectrum calculated for the **2a** was the global minimum at MP2/6-31G* but not at B3LYP/6-311+G**. Therefore, better IGLO computations have to be done on **2a** using the B3LYP/6-311+G** geometry minimum, which has four signals (1:4:2:2). If **2a** were nonrigid, the **2a** → **2f** → **2b** → **2g** → **2c** → **2g*** → **2b*** → **2f*** → **2a*** rearrangements could render the B_1-B_6 and B_7-B_9 atoms equivalent. There is a poor agreement between the averaged GIAO chemical shift values −1.2 and +25.3 ppm at B3LYP/6-311+G** and experiment. Also, the intensities of the experimental (3B, 3B, 3B) and the calculated (6B, 3B) spectra do not agree. This possibility is also not satisfactory because the experimental NMR spectrum did not change upon cooling to −60 °C.[8] The highest barrier along the **2a** → **2f** → **2b** → **2g** → **2c** → **2g*** → **2b*** → **2f*** → **2a*** pathway is 9.9 kcal/mol. But this is too high for rapid equilibration at such low temperatures.

(26) (a) Buzek, P.; Schleyer, P. v. R.; Sieber, S.; Koch, W.; Carneiro, J. W. de M.; Vancik, H.; Sunko, D. E. *J. Chem. Soc., Chem. Commun.* **1991**, 671. (b) Buzek, P.; Schleyer, P. v. R.; Vancik, H.; Sunko, D. E. *J. Chem. Soc., Chem. Commun.* **1991**, 1538.

(27) Klanberg, F.; Eaton, F. R.; Guggenberger, L. J.; Muetterties, E. L.; *Inorg. Chem.* **1967**, *6*, 1271.

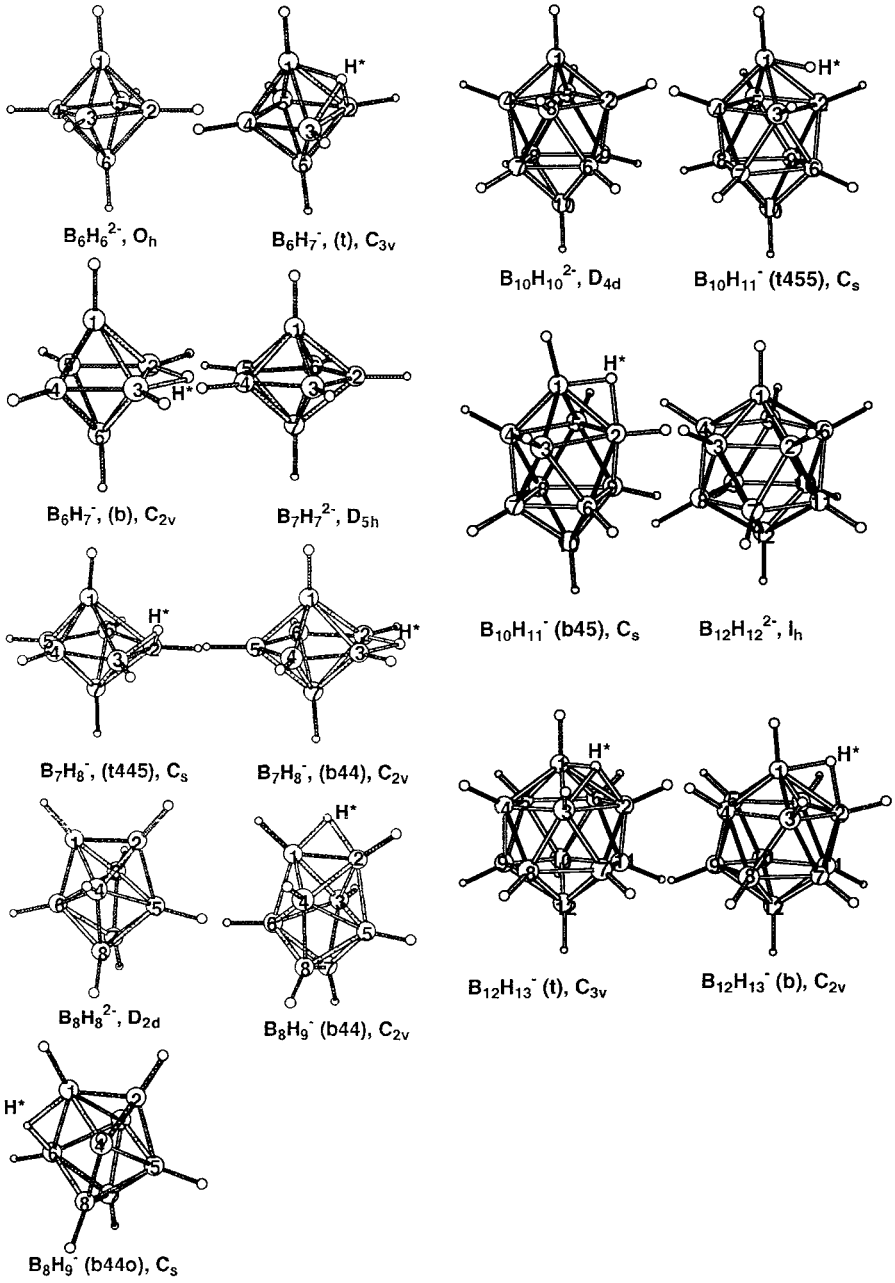

Figure 3. B3LYP/6-311+G** optimized geometries for $B_nH_n^{2-}$ and $B_nH_{n+1}^-$.

Thus, we failed to find a structure of $B_9H_{10}^-$ with a computed ^{11}B NMR spectrum in agreement with the experimental data. The reported experimental spectrum,[8] which was complicated by decomposition and the presence of other species, should be redetermined and refined.

Comparisons of the $B_nH_{n+1}^-$ Set

Figure 3 shows the key structures of the $B_nH_{n+1}^-$ anions (n = 6−8, 10, 12) optimized at the B3LYP/6-311+G(d,p) level. The energies of these species, calculated at the B3LYP/6-31G(d), B3LYP/6-311+G(d,p), and MP2/6-31G(d) levels with the B3LYP/6-31G(d) ZPE corrections are presented in Table 7. We use the structural notations suggested earlier: "t" and "b" denote tridentate capping and bidentate bridge positions, respectively, "v" indicates involvement in a terminal BH_2 group, "o" describes an "open" structure, and "B4" and "B5" designate the skeletal coordination numbers of the boron atoms bonded to H*. In general, the B3LYP data confirm the earlier single-point MP2 results.[10] We discuss here the common as well as the specific features of the $B_nH_{n+1}^-$ series (n = 6−8, 10, 12), e.g. the site preference for the additional proton, and the main changes in the $B_nH_n^{2-}$ geometries upon protonation, the proton affinities, as well as the topomerization barriers and pathways. We do not consider $B_{11}H_{11}^{2-}$ and $B_{11}H_{12}^-$ here, because of the inherent complexity of the latter system. $B_5H_5^{2-}$ is not known experimentally, and $B_5H_6^-$ (also not known) probably has an open structure unrelated to the other protonated clusters.

The two different coordinations of a boron atom to other skeletal borons in $B_nH_n^{2-}$ (n = 6−10, 12) are denoted as B4 and B5. The B4 atoms have higher negative charges and bind the additional proton in $B_nH_{n+1}^-$ more strongly than the B5 borons. The skeletal regions with the largest possible number of B4's are the preferred sites for protonation. $B_6H_7^-$ affords the simplest illustration. All boron atoms (B4) and all BB bonds in

Table 7. Data for $B_nH_n^{2-}$ and $B_nH_{n+1}^-$: Total Energies in au with Relative Energies of Isomers and Proton Affinities (PA) (Both with Scaled ZPE's[a] in kcal/mol) for the Dianions Given in Parentheses

species	type	B3LYP/6-31G(d) (rel energy)	ZPE[a] (NIMAG)	MP2/6-31G(d) (rel energy)	B3LYP/6-311+G(d,p) (rel energy)
$B_6H_6^{2-}$ (PA)	O_h	(449.0)	47.1 (0)	(445.0)	(431.9)
$B_6H_7^-$	t[b]	−153.37936 (0.0)	54.8 (0)	−152.71220 (0.0)	−153.42498 (0.0)
	b	(8.9)	54.4 (1)	(12.2)	(8.3)
$B_7H_7^{2-}$ (PA)	D_{5h}	(433.7)	56.3 (0)	(427.8)	(420.4)
$B_7H_8^-$	t445[b]	−178.84692 (0.0)	64.2 (0)	−178.07485 (0.0)	−178.89430 (0.0)
	b44	(2.6)	63.9 (1)	(2.4)	(2.2)
$B_8H_8^{2-}$ (PA)	D_{2d}	(430.4)	65.1 (0)	(425.8)	(418.6)
$B_8H_9^-$	b44[b]	−204.31991 (0.0)	73.4 (0)	−203.44864 (0.0)	−204.36928 (0.0)
	b44o	(5.1)	73.3 (0)	(9.1)	(4.8)
	TS	(8.9)	72.6 (1)	(11.3)	(8.3)
$B_9H_9^{2-}$ (PA)	D_{3h}	(415.1)	74.5 (0)	(408.1)	(403.9)
$B_9H_{10}^-$	v4[b]	−229.79516 (0.0)	81.8 (0)	−228.82269 (0.0)	−229.84573 (0.0)
	open	(0.9)	81.5 (0)	(3.0)	(−1.1)
$B_{10}H_{10}^{2-}$ (PA)	D_{4d}	(399.9)	84.7 (0)	(393.5)	(391.1)
$B_{10}H_{11}^-$	t455[b]	−255.29181 (0.0)	91.4 (0)	−254.22691 (0.0)	−255.34754 (0.0)
	b45	(1.0)	91.5 (1)	(2.1)	(0.9)
$B_{12}H_{12}^{2-}$ (PA)	I_h	(372.8)	104.8 (0)	(365.5)	(366.1)
$B_{12}H_{13}$-	t[b]	−306.29525 (0.0)	111.7 (0)	−305.03816 (0.0)	−306.35078 (0.0)
	b	(3.4)	110.9 (1)	(4.7)	(3.2)

[a] Zero-point energies scaled by 0.98 (kcal/mol), calculated at the B3LYP/6-31G(d) level. In parentheses: number of imaginary frequencies (NIMAG). [b] Total energies in hartrees. The relative energies and PA's with ZPE are given with respect to this species in kcal/mol.

$B_6H_6^{2-}$ are equivalent, but H* forms a capping bond in $B_6H_7^-$ with three B4's over an octahedron face rather than bridging a BB edge.

In the global minimum of $B_7H_8^-$ t445, H* is located over a skeletal face much closer to the two equatorial B4 atoms (B4−H* = 1.30 Å) than to the apical B5 (B5−H* = 2.15 Å). Structure b44, with H* in a symmetrical (C_{2v}) bridge position between two of the B4 atoms in the base of the pentagonal bipyramid, is only about 2 kcal/mol higher in energy than t445. The $B_8H_8^{2-}$ dianion has two geometries close in energy, *closo*-D_{2d} and *nido*-C_{2v}. The protonation of each at B4−B4 edge sites produces the most stable b44 and b44o $B_8H_9^-$ conformers. H* forms bridge bonds between two B4's.

As discussed earlier, H* in $B_9H_{10}^-$ also prefers to be located near the apical B4 atoms; the favored structures are **2a** (BH_2 group for B4) and **2b** (a capping arrangement with B4 and two B5's but lacking a B5−B5 bond). The B4's in the $B_{10}H_{10}^{2-}$ dianion are located at the polar positions. In the most stable $B_{10}H_{11}^-$ structure, t455, H* caps the B4−B5−B5 face but is closer to B4 than to the B5's. The H* interaction with one of B5's is weak; the b45 structure with H* bridging the B4−B5 edge is only 1−2 kcal/mol higher in energy than t455.

$B_{12}H_{12}^{2-}$ is the only dianion in the set which does not have any B4's in the skeleton, as only B5's are possible in I_h symmetry. In the most stable $B_{12}H_{13}^-$ structure, t, H* caps a BBB face. Structure b, with a B−H*−B bridge, is 3−5 kcal/mol higher in energy than t and is the transition state for H* migration around the skeleton. As has been shown experimentally and theoretically, $B_{12}H_{13}^-$ is not a stable species. This monoanion easily loses molecular hydrogen and forms a $B_{24}H_{23}^{3-}$ "dimer", at least formally by the interaction of $B_{12}H_{11}^-$ with $B_{12}H_{12}^{2-}$. We will discuss the mechanism of the H_2 elimination from $B_{12}H_{13}^-$ and the formation of $B_{24}H_{23}^-$ elsewhere.

The boron skeletons of the $B_nH_n^{2-}$ dianions undergo substantial deformations on protonation, and this influences the location of H* considerably. The BB bonding of borons involved in the capping and bridge bonds with H*'s are weakened, and quite large changes in geometry can result. For example, in $B_6H_7^-$, $B_7H_8^-$, and $B_8H_9^-$, the capped and bridged B4−B4 bonds are elongated by 0.05−0.15 Å (compared to the lengths in corresponding dianions). Specific BB bonds involved in H* capping arrangements, B4−B5 in $B_7H_8^-$ as well as B5−B5 in $B_{10}H_{11}^-$ and $B_{12}H_{13}^-$, are stretched by 0.17−0.25 Å to separations as large as 2.0−2.1 Å. $B_9H_{10}^-$ exhibits the largest skeletal deformation; protonation on the B4−B5−B5 face ruptures three neighboring B5−B5 bonds and transforms the *closo* boron skeleton into the *nido* form (**2b**). The B5−B5 distances in the t555 isomer (**2c**) of $B_9H_{10}^-$ are elongated to 2.39 Å from 1.91 Å in the dianion. Protonation on the B4−B5 edge of the intrinsically fluxional $B_8H_8^{2-}$ also leads to skeletal opening and the formation of the $B_8H_9^-$ b44o structure.

All the $B_nH_{n+1}^-$ species undergo facile proton migrations. The barriers for the H* shifts vary but are never high. H* prefers to move around the B4 sites, when these are available. For example, since all borons in $B_6H_6^{2-}$ are B4's, H* in $B_6H_7^-$ migrates over the entire octahedron from one face (t) to another via the edge protonated transition structures (b). The barrier is 8.3 kcal/mol at B3LYP/6-311+G**. B4's are positioned in the equatorial base of the $B_7H_7^{2-}$ bipyramid. The H* migrations in $B_7H_8^-$ include "hemisphere to hemisphere" oscillations over an B4−B4 edge, t445 → b44 → t445, with a ca. 2 kcal/mol barrier as well as face to face motions in each hemisphere over a B4−B5 edge, t445 → b45 → t445 → etc., with a 17 kcal/mol barrier. Since B4 occupies the polar positions in $B_{10}H_{10}^{2-}$, H* in $B_{10}H_{11}^-$ rotates readily around each pole region, t455 → b45 → t455, with a barrier of 1−2 kcal/mol. The movement of H* from one pole to the other (via the central region of the polyhedron) is much less facile.[10c]

The topomerizations of $B_8H_9^-$ and $B_9H_{10}^-$ occur by complicated mechanisms: the hydrogen migrations, in contrast to $B_6H_7^-$, $B_7H_8^-$, $B_{10}H_{11}^-$, and $B_{12}H_{13}^-$, are accompanied by structural changes of the boron skeletons. The $B_8H_8^{2-}$ dianion is highly fluxional; *closo*-D_{2d} and *nido*-C_{2v} conformers interconvert with a negligible barrier, only 0.1 kcal/mol. The protonated $B_8H_9^-$ species is more rigid; the barrier between the b44 $B_8H_9^-$ isomer, with a *closo*-skeleton, and b44o, with a *nido*-skeleton, is computed to be 8.3 kcal/mol (B3LYP/6-311+G**). The degenerate migration of H* in $B_8H_9^-$ from one B4−B4 edge to another around the whole skeleton, b44 → TS → b44o → TS′ → b44o′ → TS → b44′, involves the opening and closing of the boron frame. The isomerization of $B_9H_{10}^-$, discussed in detail in the previous sections, also proceeds with the skeletal opening and closing during H* migration.

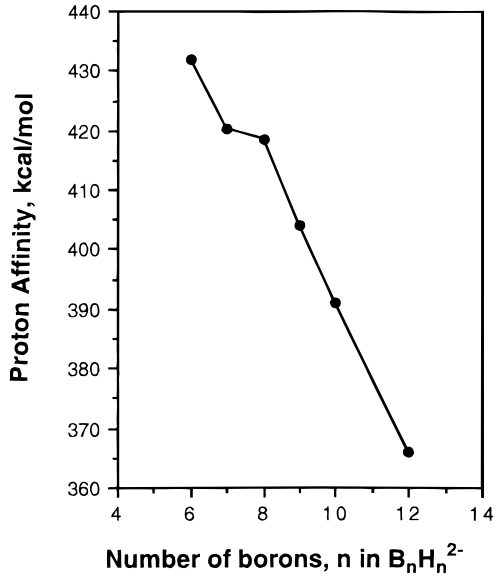

Figure 4. Proton affinities (PA) of the $B_nH_n^{2-}$ dianions decreasing generally with cluster size.

Table 8. Characteristic Vibrational Frequencies (cm^{-1}) for the Key $B_nH_n^{2-}$ and $B_nH_{n+1}^{-}$ Structures

		B−H frequencies		H* frequencies	
species	type	unscaled	scaled[a]	unscaled	scaled[a]
$B_6H_6^{2-}$		2395−2460	2306−2369		
$B_6H_7^{-}$	t	2595−2650	2499−2552	1211, 1799	1166, 1732
	b	2585−2635	2489−2538	1815, 2076	1748, 1999
$B_7H_7^{2-}$		2395−2464	2306−2373		
$B_7H_8^{-}$	t445	2573−2632	2478−2535	1790, 2079	1724, 2002
	b44	2565−2640	2470−2542	1913, 2182	1842, 2101
$B_8H_8^{2-}$		2404−2492	2315−2400		
$B_8H_9^{-}$	b44	2580−2635	2485−2538	1766, 2132	1701, 2053
	b44o	2567−2635	2472−2538	1840, 2038	1772, 1963
$B_9H_9^{2-}$		2455−2528	2364−2434		
$B_9H_{10}^{-}$	v4	2603−2652	2507−2554	2536, 2548	2442, 2454
	open	2594−2662	2498−2564	1135, 2012	1093, 1938
$B_{10}H_{10}^{2-}$		2482−2552	2390−2458		
$B_{10}H_{11}^{-}$	t455	2601−2668	2505−2569	1263, 2093	1216, 2016
	b45	2562−2656	2467−2558	1730, 2077	1666, 2000
$B_{12}H_{12}^{2-}$		2509−2572	2416−2477		
$B_{12}H_{13}^{-}$	t	2619−2664	2522−2565	1302, 1717	1254, 1653
	b	2592−2661	2496−2563	1661, 1944	1600, 1872

[a] The scaling factor is 0.963.

In $B_{12}H_{13}^{-}$, the additional proton can move from one equivalent B5−B5−B5 icosahedron face to another via a B5−B5 edge and 3.2 kcal/mol barrier (B3LYP/6-311+G**). H* also can form a weak $B_{12}H_{11}^{-}$. H_2 complex; this can then lose molecular hydrogen (see above). However, the geometry of the icosahedral boron skeleton changes little in these processes, except for the elongation of B−B distances involved with the H* bonding.

At the B3LYP/6-311+G(d,p) level, the proton affinities (PA) for the $B_nH_n^{2-}$ dianions decrease from 432 kcal/mol for $B_6H_6^{2-}$ to 366 kcal/mol for $B_{12}H_{12}^{2-}$ (Table 7). These differences in PA values are due to two factors. The first is related to the size of the dianions (Figure 4). Even at the diffuse function-augmented B3LYP/6-311+G(d,p) level, many of the occupied eigenvalues of the dianions are positive (unbound), due to Coulomb repulsion. This electrostatic problem, less severe for the larger dianions, is alleviated upon protonation; the inverse dependence of the PA's with the size of the system (Figure 4) results.

Table 9. Selected Interatomic Distances (Å) for $B_nH_n^{2-}$ and $B_nH_{n+1}^{-}$ (n = 6−8) at the B3LYP/6-311+G** Level, with the Atom Numbering Shown in Figure 3

		$B_6H_7^{-}$			$B_7H_8^{-}$			$B_8H_9^{-}$	
	$B_6H_6^{2-}$	t	b	$B_7H_7^{2-}$	t445	b44	$B_8H_8^{2-}$	b44	b44o
B1B2	1.737	1.881	1.821	1.830	2.085	1.911	1.616	1.673	1.686
B1B3								1.852	1.821
B1B4			1.694			1.797			
B1B5					1.779	1.801			
B1B6					1.753		1.709	1.767	1.812
B2B3			1.790	1.657	1.746	1.733			1.776
B3B4		1.707	1.730		1.678	1.668			
B4B5		1.727	1.737		1.646	1.627	1.909	1.882	1.881
B6B8							1.822	1.764	2.076
B7B2					1.806				
B7B4					1.841				
B7B5					1.801				1.720
B7B8								1.628	1.667
B8B4								1.703	1.700
BH*		1.425	1.300		1.301	1.276		1.292	1.302
					2.147				

Table 10. Selected Interatomic Distances (Å) for $B_nH_n^{2-}$ and $B_nH_{n+1}^{-}$ (n = 10 and 12) at the B3LYP/6-311+G** Level, with the Atom Numbering Shown in Figure 3

		$B_{10}H_{11}^{-}$			$B_{12}H_{13}^{-}$	
	$B_{10}H_{10}^{2-}$	t455	b45	$B_{12}H_{12}^{2-}$	t	b
B1B2	1.703	1.824	1.775	1.786	1.956	1.895
B1B3			1.779			
B1B4		1.708	1.720			1.780
B2B3	1.842	2.048	1.927			1.894
B3B4		1.794	1.812			1.753
B3B7		1.804	1.778		1.800	
B3B6	1.822		1.765			
B4B5		1.874				1.851
B4B8		1.797	1.800			1.775
B6B7		1.865				
B6B9			1.981			
B7B8		1.817	1.857		1.796	
B10B6		1.713	1.698			1.765
B10B7		1.684				
B10B8		1.715	1.713			
B12B7					1.786	1.793
B12B8					1.766	1.782
B12B9					1.793	
BH*		1.291	1.297		1.393	1.310
		1.502	1.300			

The second factor influencing the $B_nH_n^{2-}$ PA's is the coordination at the protonation sites. The number of B4 atoms in $B_nH_{n+1}^{-}$, to which the extra proton is bound, also decreases with increasing cluster size. Thus, H* is connected to three B4 atoms in $B_6H_7^{-}$, to two B4 atoms in $B_7H_8^{-}$ and $B_8H_9^{-}$, to one B4 in $B_9H_{10}^{-}$ and $B_{10}H_{11}^{-}$ but only to B5 atoms in $B_{12}H_{13}^{-}$. Since the H* binding energy to B4 is greater than to B5, stepwise PA decreases from $B_nH_n^{2-}$ to $B_{n+1}H_{n+1}^{2-}$ (which average 11 kcal/mol) can be expected. The only exception, the ca. 2 kcal/mol decrease from $B_7H_7^{2-}$ to $B_8H_8^{2-}$ apparent in Figure 4, may be attributed to the similar B4−B4−B5 coordination at the protonation sites.

The calculated B−H stretching frequencies and those corresponding to the vibrations involving H* are presented in Table 8. The B−H frequencies generally are shifted to the blue by 100−200 cm^{-1} upon protonation. This reflects the 0.01−0.02 Å shortening of the B−H distances in $B_nH_{n+1}^{-}$ as compared to those in $B_nH_n^{2-}$ (Tables 9 and 10). Protonation also leads to new vibrations related to the capping and the bridge bonds involving H*. The characteristic frequencies are 1200 and 1700 cm^{-1} for the capping H*−BBB bonds and are in the 1700−1800 and 2000 cm^{-1} ranges for the bridge B−H*−B bonds.

Conclusions

Both computed energies and NMR chemical shifts confirm that **1a** (D_{3h}) is the most stable $B_9H_9^{2-}$ dianion structure. The "opening−closing" of the trigonal prism bases of the boron skeleton has a small barrier. In contrast, scrambling of the boron atoms via the single and double DSD mechanisms requires relatively large activation energies (28.38 and 21.27 kcal/mol, respectively, at the B3LYP/6-311+G**+ ZPE level) and should not be observable on the dynamic NMR time scale.

The most stable C_s **2b** configuration for the $B_9H_{10}^-$ monoanion has an additional H* involved in a nonsymmetric four-center bond above the open face of $B_9H_9^{2-}$, forming a nonsymmetrical cap with one four-coordinated and two three-coordinated borons. The isomer **2a**, with a BH_2 group at the four-coordinated capping boron atom, is slightly less stable. The highest barrier along the pathway of the **2a** → **2f** → **2b** → **2g** → **2c** → **2g*** → **2b*** → **2f*** → **2a*** intramolecular rearrangement is 9.9 kcal/mol (B3LYP/6-311+G** + ZPE). This calculated barrier as well as the IGLO chemical shifts are not consistent with the reported ^{11}B NMR spectral interpretation and exclude the **2c** structure with C_{3v} symmetry. The NMR spectrum and its interpretation[8] needs to be reexamined. We hope that our calculations will stimulate further experimental studies of the $B_9H_{10}^-$ anion. X-ray structural analysis would be particularly revealing.

The boron skeletons of the $B_nH_{n+1}^-$ species distort from the unprotonated $B_nH_n^{2-}$ geometries due to the influence of the extra hydrogen. This distortion is greatest when polyhedral rings open as in $B_8H_9^-$ and $B_9H_{10}^-$. The fluxionality of $B_nH_{n+1}^-$ occurs via rapid hydrogen migration rather than by transformations of the boron framework. In $B_6H_7^-$ H* migrates over the whole octahedron. In $B_7H_8^-$, the additional hydrogen H* rotates easily over one side of the bipyramid. However, in $B_8H_9^-$ and in $B_9H_{10}^-$, the H* migration is accompanied by a skeletal DSD rearrangement. The polyhedron pole region in $B_{10}H_{11}^-$ is most favorable for the H* migration.

The proton affinity (PA) for the *closo*-borane dianions decreases with increasing cluster size. This is due to electrostatic effects related to the size of the dianions (Figure 4) but also to the coordination number at the protonation sites.

Acknowledgment. This work was supported jointly by the Deutsche Forschungsgemeinschaft and the Russian Academy of Sciences, as well as by the Fonds der Chemischen Industrie, the Stiftung Volkswagenwerk, and Convex Computer Corp. We thank Professor W. Kutzelnigg and Dr. M. Schindler for the Convex version of the IGLO program as well as Dr. M. Bühl for helpful discussions. K.N. thanks Deutscher Akademischer Austauschdienst (DAAD) for a doctoral fellowship.

IC970940T